High Precision Angular Measurement via Dual Imaging Detectors

Hai Yu, *Member, IEEE*, Qiuhua Wan, Ying Sun, Xinran Lu, and Changhai Zhao

***Abstract*— This paper proposes a novel error compensation arithmetic based on dual imaging detectors which can eliminate errors caused by grating eccentricity. First, we built an error model and analyzed the error change current. Furthermore, we deduced the error compensation arithmetic and established the dual-image-detector-based method. Finally, we conducted a series of experiments to test the performance of this arithmetic. The test results showed that we achieved a standard error deviation of 6.33″ and grating diameter of only 38 mm. This arithmetic outperforms the single detector and is far superior to the traditional method. The results presented here may provide a theoretical foundation for further research on angle-displacement measurement.**

***Index Terms*— Angular measurement, high precision, dual imaging detectors.**

I. Introduction

THE photoelectric encoder is a measurement device which transforms rotations to digital angular values via photoelectric conversion. It is utilized in a variety of industries and is favored for its high resolution and precision [1]–[5]. Studies on angle displacement measurement tend to prioritize smaller size, higher resolution, and higher precision. Traditional methods realize angle measurement based on moiré fringe, and are relatively imprecise when using a small-size grating [6].

When grating diameter is below 40 mm, measurement methods based on moiré fringe can achieve up to 16-bit resolution but no better than 30″ precision [7], [8]. In recent years, non-diffractive beams have been used to realize high resolution increment angle measurement [9], [10], but these devices cannot realize absolute measurement. New angle measurements with enhanced accuracy and resolution are yet in demand. Advancements in digital image processing technology [11]–[17] have yielded image detectors with better angle measurement, but it is still very challenging to secure higher precision with small-size grating. Image type encoder researchers in the United States [18], [19], Serbia [20], Japan [21], Spain [22], Korea [23], China [24], [25], and other countries have made remarkable achievements in this regard.

Manuscript received March 19, 2019; revised May 4, 2019; accepted May 5, 2019. Date of publication May 8, 2019; date of current version August 6, 2019. This work was supported in part by the National Natural Science Foundation of China under Grant 51605465 and in part by the Science and Technology Development Program of Jilin Province under Grant 20180520184JH. The associate editor coordinating the review of this paper and approving it for publication was Dr. Qiang Wu. *(Corresponding author: Hai Yu.)*

The authors are with the Changchun Institute of Optics, Fine Mechanics and Physics, Chinese Academy of Sciences, Changchun 130033, China (e-mail: yuhai@ciomp.ac.cn).

Digital Object Identifier 10.1109/JSEN.2019.2915579

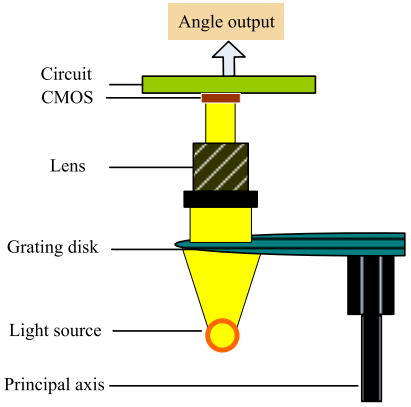

Fig. 1. Measurement principle used in previous study.

There have been relatively few studies, however, on subdivision and compensation methods based on image detectors.

In a previous study, we used a single imaging detector to achieve angular measurement, as shown in Figure 1 [26]. Also, we proposed a novel subdivision arithmetic [27]. However, grating eccentricity caused substantial error which we were unable to fully eliminate.

This paper reports an effective error-compensation arithmetic which eliminates eccentricity error. We built the corresponding mathematical model and deduced the error-compensation arithmetic, then we designed a test encoder with diameter of 52 mm and length of 55 mm which yielded 8,192-fold angle subdivision between 256 “reference lines”.

The remainder of this paper is organized as follows. In Section 2, the principle of angular measurement subdivision arithmetic is proposed. In Section 3, grating eccentricity error is analyzed. In Section 4, the proposed error-compensation arithmeticis detailed based our analyses of eccentricity. Section 5 details the designing of device. Section 6 presents a series of test results. Conclusions are provided in Section 7.

II. Angular Measurement Subdivision Arithmetic

Grating is an important component in angle displacement measurement. In a grating, there are 2^N reference lines which are concentric and equal in width. The angle subdivision value can be obtained by a subdivision arithmeticbased on the image of two adjacent reference lines collected by an image detector. The principle of the grating is shown in Figure 2.

An amplified image of two adjacent reference lines is shown on the right-hand side of Figure 1. *L1* and *L2* are two adjacent reference lines; *L3* is the detection line of the image detector.

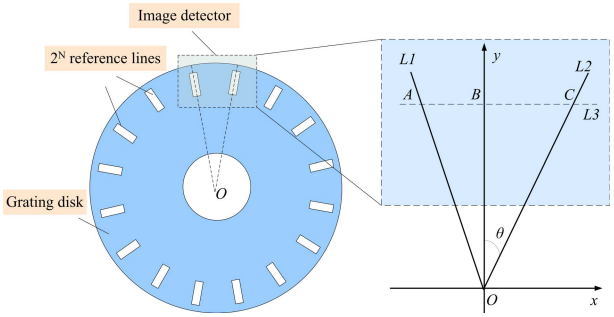

Fig. 2. Two adjacent reference lines.

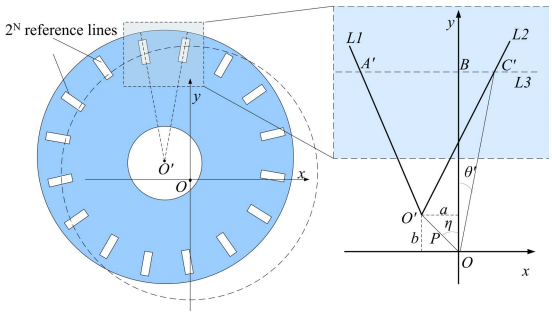

Fig. 3. Grating with eccentricity.

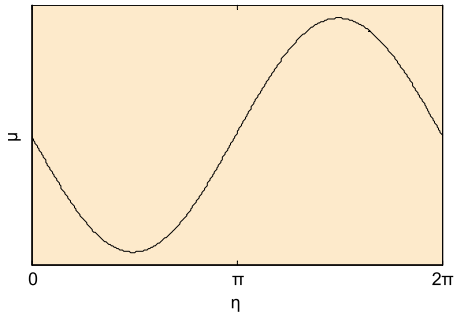

Fig. 4. Curve of error μ.

Dots A and B are the centroid of $L1$ and $L2$ in the direction of $L3$; O is the circle center of the grating disk. The length of BO is the length of the image detector. We built coordinate system xoy, where the distance between $L2$ and the y-coordinate is, in the point C, is BC. Because $L3$ is settled into the image, BO is constant. θ can be calculated by Formula (1):

$$\theta = \arctan(\frac{BC}{BO}) \tag{1}$$

Because of the "reference lines" have a certain width, precisely finding out the center of "reference lines" is the key of subdivision. We fitted every "reference lines" by two-fold linear function based on the least square method accordingly. The two-fold function is expressed as follows:

$$f(x) = ax^2 + bx + c \tag{2}$$

Where, {a, b, c} are coefficients. To fit one subdivision reference line, the difference of squares sum between f(x) and pixel values p(x) must reach minimum in window $\{n\}$, as shown in formula (3).

$$Min = \sum_{x \in n} [f(x) - p(x)]^2 \tag{3}$$

By calculating, the center of one subdivision reference line is the extreme point of $f(x)$, as shown in Formula (4).

$$U = -\frac{b}{2a} \tag{4}$$

Using Formula (4), we can get the center dot A and dot C, and achieve angular measurement subdivision.

III. Error Analysis

When the grating is not concentric with the true center, the eccentricity will cause measurement error as shown in Figure 3.

Eccentricity is marked as P in Figure 3. Grating centre moves to O', where O is the center of revolution. The intersection angle between the y-coordinate and eccentricity is η. At this point, dots A' and C' are the intersections between $L1$, $L2$, and $L3$; BC is the distance between $L2$ and the y-coordinate, in point C.

There are

$$BC' = BC\frac{(BO - b)}{BO} - a \tag{5}$$

$$\theta' = \arctan(\frac{BC'}{BO}) \tag{6}$$

$$a = P\sin\eta$$

$$b = P\cos\eta \tag{7}$$

Set μ is error which can be expressed as follows:

$$\tan\mu = \tan(\theta - \theta') = \frac{\tan\theta - \tan\theta'}{1 - \tan\theta\tan\theta'} \tag{8}$$

Plugging Formula (1) and Formula (6) into Formula (8) yields

$$\tan\mu = \frac{\frac{BC}{BO} - \frac{BC'}{BO}}{1 - \frac{BC \cdot BC'}{BO \cdot BO}} = \frac{BC \cdot BO - BC' \cdot BO}{BO^2 - BC \cdot BC'} \tag{9}$$

Thus we can calculate μ by Formula (10):

$$\mu = \arctan[\frac{BC \cdot P\cos\eta - BO \cdot P\sin\eta}{BO^2 - BC^2 + BC^2 \cdot P\cos\eta / BC + BC \cdot P\sin\eta}] \tag{10}$$

When θ is invariable, BC and BO also are invariable and the change current of eccentric-angle η is as shown in Figure 4. When $\eta = 0, \pi, 2\pi$, $|\mu|$ is minimal; when $\eta = \pi/2, 3\pi/2$, $|\mu|$ is maximal.

IV. Error Compensation Arithmetic

We next rotated the xoy-coordinate to angle β as shown in Figure 5.

After rotation, xoy changes to $x'oy'$. A'' and C'' are the intersection between detection lines $L3$ and $L1$ with $L2$. The distance between $L2$ and the y-coordinate is BC''. In the

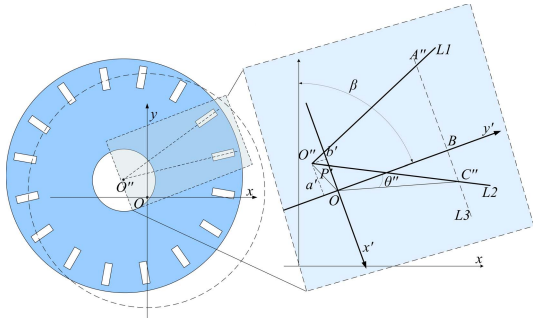

Fig. 5. Grating with rotation β.

new coordinate system $x'oy'$, a' and b' can be calculated as follows:

$$\begin{aligned} a' &= a\cos\beta - b\sin\beta \\ b' &= b\cos\beta - a\sin\beta \end{aligned} \tag{11}$$

In accordance with section 3, the errors are inverse when angle difference is π. So, let $\beta = \pi$, then $a' = -a$, $b' = -b$. BC'' can be calculated as follows:

$$BC''\big|_{\beta=\pi} = BC\frac{(BO+b)}{BO} + a \tag{12}$$

Adding Formula (12) to Formula (5) yields the following:

$$\begin{aligned} BC' + BC''\big|_{\beta=\pi} &= BC\frac{(BO-b)}{BO} - a + BC\frac{(BO+b)}{BO} + a \\ &= 2\cdot BC \end{aligned} \tag{13}$$

Which allows us to acquire BC by the addition of BC' and BC'' and thus eliminate the error caused by eccentricity. The full errors compensate arithmetic is as follows:

$$\theta = \arctan\left(\frac{BC' + BC''\big|_{\beta=\pi}}{2\cdot BO}\right) = \arctan\left(\frac{BC}{BO}\right) \tag{14}$$

From Formula (14), we next used two image detectors to reduce the eccentricity error.

V. Device Designing

We designed a test device to test the measurement capacity of the error-compensation algorithm. The principle of the dual image detectors setup is illustrated in Figure 6. In position, two image detectors are placed in the diameter of the grating and the intersection angle of the image detectors is π (From Formula (13)).

Parallel light is transmitted across the grating and passes into the lens. The grating patterns are amplified 5× and projected on image detectors #1 and #2. The circuit both collects the pixel-data of dual image detectors and calculates the angle data via Formula (14). In figure 6, the two image detectors must be parallel to each other, but not strictly. The installation angle of image detector has little influence on measurement [28].

There are 2^8 "reference lines" on the circumference which are used to achieve subdivision. The grating is shown in figure 7. We set up three Region of Interests (ROI) [29] on the image detectors to reduce the quantities of pixels.

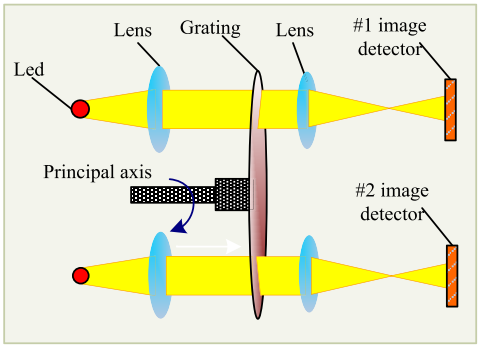

Fig. 6. Dual image detector-based angular measurement with two optical systems.

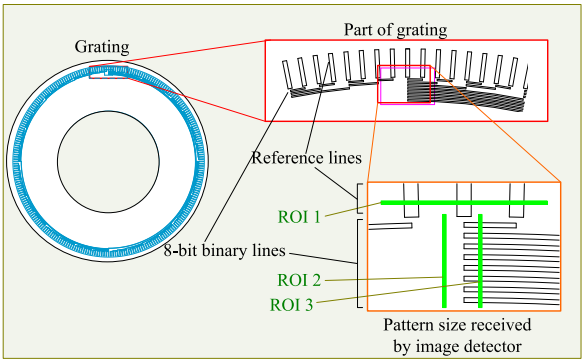

Fig. 7. The design of grating.

Among them, ROI-1 is used to read out the pixels-data for subdivision, ROI-2 and ROI-3 is used to discriminate binary marker lines. Furthermore, in #2 image detector, only ROI-1 need be read out.

ROI-3 of #1 image detector is subsidiary binary marker lines reading. In normally, ROI-2 can read out binary data directly, the binary data read by ROI-2 is "0000 0100". When ROI-2 is in critical position (close to a reference line), we will read binary marker lines by using ROI-3.

For error compensation, we get BC′ value by ROI-1 of #1 image detector, and get BC″ value by #2 image detector. Then we do the arithmetic of Formula (14).

The test device is shown in Figure 8. There are two optical systems called #1 and #2. The grating diameter is 38mm. The length of the device is 55mm with the diameter is 52mm. The wavelength of LED is 850nm. The focal length of the lens is 4mm. The image detector is an area arrays CMOS sensor produced by "ON Semiconductor".

VI. Test

A. Subdivision Test

The collected image is shown in figure 9.Figure 9(a) is the image of ROI-1 in #1 detector, (b) and (c) are images of ROI-2, ROI-3 in #1 detector. (d) is the image of ROI-1 in #2 detector. In each image of figure 9(a) and (d), there are four reference lines, and figure 9(b) and (c) are used to calculate "Binary data". In this position, ROI-2 is not in critical position (not close to a reference line), so we use figure 9(b) and the "Binary

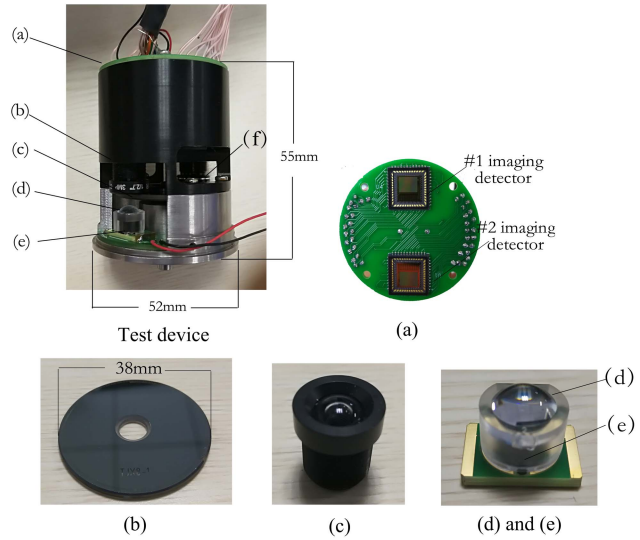

Fig. 8. Test device. (a) Circuit, (b) Lens, (c) Grating disk, (d) Lens, (e) Led (inside), (f) #2 optical system.

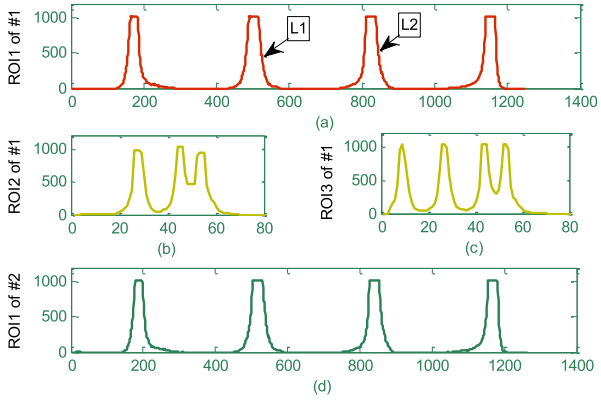

Fig. 9. The collected images. (a), (b) and (c) are collected by #1 detector; (d) is collected by #2 detector.

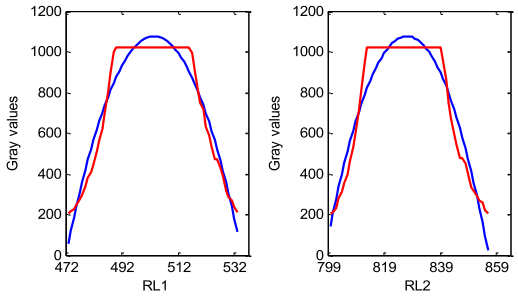

Fig. 10. Two reference lines. (The red lines are the curves of two-fold function; we get reference-line-centre by $-b/2a$.)

data" is "00101100". We can see the images are perfect for the test. In figure 9(a), we get two reference lines ($L1$ and $L2$). Using formula (4) to calculate the centre of $L1$, $L2$. The results are shown in figure 10. By calculate, the centre values are $A = 607.6078$ and $C = 826.1546$. Then by formula (14), we can get the subdivision values after errors compensation.

We let $2^n = 2^{12}$, $2^n = 2^{13}$ and $2^n = 2^{14}$ in proper order, then turned the axis of test device and observe the carry of output data. It all be correct carry when $2^n = 2^{12}$, and $2^n = 2^{13}$. But when $2^n = 2^{14}$, the output data are not steady. These shows: we can achieve 2^{13}-fold subdivision in this test.

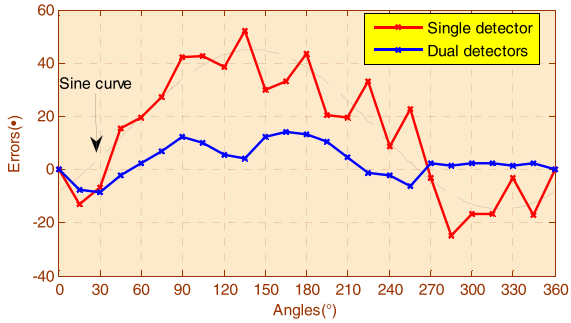

Fig. 11. Errors in single and dual detectors. (With mean square, single detector is 22.73″; dual detector is 6.63″.)

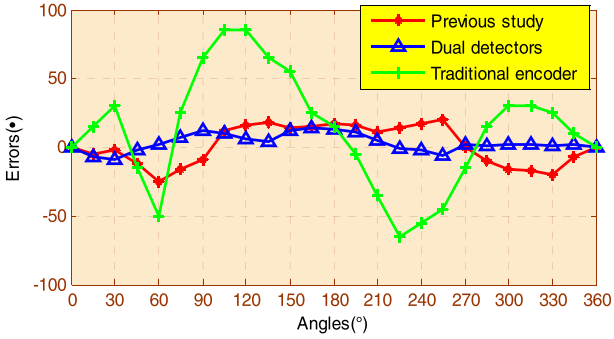

Fig. 12. Error comparison. (with mean square, previous result is 14.3″, ours is 6.63″, and traditional encoder is only 41.5″.)

B. Precision Test

We measured the angle-errors of the test device with a 24-polyhedron and autocollimator, and the grating was deviated designedly. For comparison, we first used a single detector and tested the measurement errors. The single detector errors were marked with a red line in Figure 11 with a mean square error of 22.73″. There is a one-time sine wave in this error curve as-influenced by eccentricity.

When using dual detectors, the errors were marked by the blue line in Figure 11 where the mean square error is 6.33″. The precision was better when using the dual detector and the one-time harmonic errors were decreased.

In Figure 12, compared to the results we proposedin *Applied Optical* [26] using a single image detector (blue line), the mean square error is only 14.3″. The errors of several traditional encoders (Moiré figure measurement) are marked with a green line in Figure 12 with the mean square of 41.5″. In effect, the dual image detector substantially enhances the device's precision. The performance on this measurement test is more excellent compared to traditional angle measurement.

VII. Conclusions

This paper proposed an effective arithmetic to eliminate eccentricity error. Tests confirmed that proposed arithmetic yields 6.33″ precision in a 1280 × 1024 image detector with

grating diameter of only 38 mm. We hope that the results provided here represent a sound technological foundation for small-size angular measurement.

REFERENCES

[1] K. Hane, T. Endo, Y. Ito, and M. Sasaki, "A compact optical encoder with micromachined photodetector," *J. Opt. A, Pure Appl. Opt.*, vol. 3, no. 3, p. 191, 2001.

[2] K. Hane, T. Endo, M. Ishimori, Y. Ito, and M. Sasaki, "Integration of grating-image-type encoder using Si micromachining," *Sens. Actuators A, Phys.*, vol. 97, pp. 139–146, Apr. 2002.

[3] F. Liu, W. Wang, L. Wang, and P. Feng, "Error analyses and calibration methods with accelerometers for optical angle encoders in rotational inertial navigation systems," *Appl. Opt.*, vol. 52, no. 32, pp. 7724–7731, 2013.

[4] H. B. Zhang, Q. H. Wan, S. J. Wang, H. Yu, and L. H. Liang, "Installation error control of dynamic measurement for small photoelectric encoder," *Chin. Opt. Precis. Eng.*, vol. 24, no. 7, pp. 1655–1660, 2016.

[5] H. Yu, Q.-H. Wan, X.-R. Lu, C.-H. Zhao, and L.-H. Liang, "Calibration of dynamic precision for measurement platform of photoelectric encoder," (in Chinese), *Opt. Precis. Eng.*, vol. 24, no. 11, pp. 2704–2769, 2016.

[6] K. Patorsky and M. Kujawinska, *Handbook of the Moiré Fringe Technique*. Amsterdam, The Netherlands: Elsevier, 1993.

[7] Q.-H. Wan, Y. Sun, S.-J. Wang, R.-H. She, X.-R. Lu, and L.-H. Liang, "Design for spaceborne absolute photoelectric encoder of dual numerical system," (in Chinese), *Opt. Precis. Eng.*, vol. 17, pp. 52–57, Jan. 2009.

[8] F. Deng, J. Chen, Y. Wang, and K. Gong, "Measurement and calibration method for an optical encoder based on adaptive differential evolution-Fourier neural networks," *Meas. Sci. Technol.*, vol. 24, Apr. 2013, Art. no. 055007.

[9] F. P. Quintián, N. Calarco, A. Lutenberg, and J. Lipovetzky, "Performance of an optical encoder based on a nondiffractive beam implemented with a specific photodetection integrated circuit and a diffractive optical element," *Appl. Opt.*, vol. 54, no. 25, pp. 7640–7647, 2016.

[10] D. Hopp *et al.*, "Diffractive incremental and absolute coding principle for optical rotary sensors," *Appl. Opt.*, vol. 50, no. 26, pp. 5169–5177, 2011.

[11] A. Lutenberg and F. Perez-Quintián, "Optical encoder based on a nondiffractive beam III," *Appl. Opt.*, vol. 48, no. 27, pp. 5015–5024, 2009.

[12] W. Luo, Y. Zhang, A. Feizi, Z. Göröcs, and A. Ozcan, "Pixel super-resolution using wavelength scanning," *Light Sci. Appl.*, vol. 5, Apr. 2016, Art. no. e16060.

[13] J. Qin, R. M. Silver, B. M. Barnes, H. Zhou, R. G. Dixson, and M. Henn, "Deep subwavelength nanometric image reconstruction using Fourier domain optical normalization," *Light Sci. Appl.*, vol. 5, Feb. 2016, Art. no. e16038.

[14] S. Witte, V. T. Tenner, D. W. Noom, and K. S. Eikema, "Lensless diffractive imaging with ultra-broadband table-top sources: From infrared to extreme-ultraviolet wavelengths," *Light Sci. Appl.*, vol. 3, p. e163, Mar. 2014.

[15] V. J. Cadarso, S. Chosson, K. Sidler, R. D. Hersch, and J. Brugger, "High-resolution 1D moirés as counterfeit security features," *Light Sci. Appl.*, vol. 2, p. e86, Jul. 2013.

[16] A. C. Sobieranski *et al.*, "Portable lensless wide-field microscopy imaging platform based on digital inline holography and multi-frame pixel super-resolution," *Light Sci. Appl.*, vol. 5, p. e346, Oct. 2015.

[17] V. Bianco, P. Memmolo, M. Paturzo, A. Finizio, B. Javidi, and P. Ferraro, "Quasi noise-free digital holography," *Light Sci. Appl.*, vol. 5, Sep. 2016, Art. no. e16142.

[18] D. B. Leviton and B. J. Frey, "Ultra-high resolution, absolute position sensors for cryostatic applications," *Proc. SPIE* , vol. 4850, pp. 776–787, Mar. 2003.

[19] D. B. Leviton and M. S. Garza, "Recent advances and applications of NASA's new ultrahigh-sensitivity absolute optical pattern recognition encoders," *Proc. SPIE*, vol. 4091, pp. 375–384, Oct. 2003.

[20] J. S. Bajić, D. Z. Stupar, B. M. Dakić, M. B. Živanov, and L. F. Nagy, "An absolute rotary position sensor based on cylindrical coordinate color space transformation," *Sens. Actuators A, Phys.*, vol. 213, pp. 27–34, Jul. 2014.

[21] Y. Sugiyam *et al.*, "A 3.2 kHz, 14-bit optical absolute rotary encoder with a CMOS profile sensor," *IEEE Sensors J.*, vol. 8, no. 8, pp. 1430–1436, Aug. 2008.

[22] M. Tresanchez, T. Pallejà, M. Teixidó, and J. Palacín, "Using the image acquisition capabilities of the optical mouse sensor to build an absolute rotary encoder," *Sens. Actuators A, Phys.*, vol. 157, pp. 161–167, Jan. 2010.

[23] J.-A. Kim, J. W. Kim, C.-S. Kang, J. Jin, and T. B. Eom, "Absolute angle measurement using a phase-encoded binary graduated disk," *Measurement*, vol. 80, pp. 288–293, Feb. 2016.

[24] Y.-N. Wang, B. Yaun, and X.-X. Ni, "Subdivision technique of absolute angular encoder using array detector," (in Chinese). *Zhejiang Univ. (Eng. Sci.)*, vol. 45, pp. 370–374, Feb. 2011.

[25] L. L. Qi and W. Qiuhua, "Angle-measurement technology of an optical pattern rotary encoder and its hardware implementation," (in Chinese). *Acta Opt. Sinica*, vol. 33, no. 4, 2013, Art. no. 0412001.

[26] H. Yu, Q. Wan, X. Lu, Y. Du, and S. Yang, "Small-size, high-resolution angular displacement measurement technology based on an imaging detector," *Appl. Opt.*, vol. 56, no. 3, pp. 755–760, 2017.

[27] H. Yu, Q. Wan, X. Lu, C. Zhao, and Y. Du, "A robust sub-pixel subdivision algorithm for image-type angular displacement measurement," *Opt. Laser. Eng*, vol. 100, pp. 234–238, Jan. 2018.

[28] H. Yu, W. Q. Hua, C. h. Zhao, L, H, Liang, and Y. C. Du, "A high-resolution subdivision algorithm for photographic encoders and its error analysis," *Acta Opt. Sinica*, vol. 37, no. 3, 2017, Art. no. 0312001.

[29] Literature Distribution Center for ON Semiconductor, New York, NY, USA. (2013). *VITA 1300 1.3 Megapixel 150 FPS Global Shutter CMOS Image Sensor*. [Online]. Available: http://onsemi.com

Hai Yu (M'87) received the Ph.D. degree from the Changchun Institute of Optics, Fine Mechanics and Physics, Chinese Academy of Sciences, in 2014.

He is an Associate Research Fellow of CIOMP. His research interests have been in the area of electro-optical displacement precision measurement.

Qiuhua Wan, photograph and biography not available at the time of publication.

Ying Sun, photograph and biography not available at the time of publication.

Xinran Lu, photograph and biography not available at the time of publication.

Changhai Zhao, photograph and biography not available at the time of publication.